Sugar beet cold-induced PMT5a and STP13 carriers are poised for taproot proton-driven plasma membrane sucrose and glucose import

Antonella Reyer[1], Nadia Bazihizina[1,2], Sönke Scherzer[1], Justyna Jaślan[1,3], Nadine Schäfer[1], Dawid Jaślan[1,4], Tracey Ann Cuin[1,5], Khaled A.S. Al-Rasheid[6], Ahmed H. Alfarhan[6], Saleh A. Alquraishy[6], Frank Ludewig[7], Wolfgang Koch[7], Karsten Harms[8], Dirk Becker[1], Thomas D. Mueller[1], Benjamin Pommerrenig[9], H. Ekkehard Neuhaus[9], Irene Marten[1], Rainer Hedrich[1*]

[1] Molecular Plant Physiology and Biophysics, University of Würzburg, 97082 Würzburg, Germany

[2] Department of Agrifood Production and Environmental Sciences, Università degli Studi di Firenze, Viale delle Idee 30, 50019 Sesto Fiorentino, Florence, Italy

[3] BPMP, Univ Montpellier, CNRS, INRAE, Institut Agro, Montpellier, France

[4] Walther Straub Institute of Pharmacology and Toxicology, Faculty of Medicine, Ludwig Maximilians-Universität, 80336 Munich, Germany

[5] Biological Sciences, School of Natural Sciences, University of Tasmania, Hobart, TAS, 7005 Australia

[6] College of Science, King Saud University, 11451 Riyadh, Saudi Arabia

[7] KWS SAAT SE, Einbeck, Germany

[8] Südzucker AG, Central Department for Research, Development, and Service, 67283 Obrigheim/Pfalz, Germany

[9] Plant Physiology, University of Kaiserslautern, 67663 Kaiserslautern, Germany

*Author for correspondence: Rainer Hedrich (hedrich@botanik.uni-wuerzburg.de)

Summary

- As the major sugar-producing crop in the northern hemisphere, sugar beet taproots store sucrose at a concentration of about 20 %. While the vacuolar sucrose loader TST has already been identified in the taproot, sugar transporters mediating sucrose uptake across the plasma membrane of taproot parenchyma cells remained unknown.
- We electrophysiologically examined taproots for proton-coupled sugar uptake and identified potentially involved transporters by transcriptomic profiling. After cloning, the transporter features were studied in the heterologous *Xenopus laevis* oocyte expression system using the two-electrode voltage clamp technique. Insights into the structure were gained by 3D homology modeling.
- As with glucose, sucrose stimulation of taproot parenchyma cells caused inward H^+-fluxes and plasma membrane depolarization, indicating a sugar/proton symport mechanism. As one potential candidate for sugar uploading, the BvPMT5a was characterized as a H^+-driven low-affinity glucose transporter, which does not transport sucrose. BvSTP13 operated as a high-affinity H^+/sugar symporter, transporting glucose and to some extent sucrose due to a binding cleft plasticity. Both transporter genes were upregulated upon cold exposure, with the transport capacity of BvSTP13 being more cold-resistant than BvPMT5a.
- Identification of BvPMT5a and BvSTP13 as taproot sugar transporters could improve breeding of cold-tolerant sugar beet to provide a sustainable energy crop.

Key words: cold, glucose, plasma membrane transport, PMT5a, proton-driven sugar transport, STP13, sucrose, sugar beet (*Beta vulgaris*)

52 **Introduction**

53 Sugar beet (*Beta vulgaris*) and sugarcane (*Saccharum officinarum*) together account for the
54 world's sugar production. Industrial production of sugar from the sugar beet taproot began in
55 the early nineteenth century and since then, breeding has increased the sugar content from 8%
56 to about 21 %. From the late 1970s to the present, plant scientists have been trying to identify
57 the transport proteins that translocate sucrose from the sugar factories in the leaf to its final
58 depot in the taproot. In the early days of sugar beet (*Beta vulgaris*) research, sucrose transport
59 was examined in taproots, leaf discs and plasma membrane-enriched vesicles (Wyse, 1979;
60 Bush, 1989; Sakr *et al.*, 1993). Translocation of sucrose against its concentration gradient
61 requires metabolic energy. The first *in vitro* evidence for a proton-driven sucrose symport,
62 which uses the proton motive force (PMF) as a secondary energy source for solute uphill
63 transport, was provided by Bush (1989). Sucrose import was also found very sensitive to
64 changes in electrical membrane potential as well as to orthovanadate, an inhibitor of the H^+-
65 ATPase, whose H^+ pumping ability is required to keep the resting membrane voltage
66 hyperpolarized, and to retain the inward H^+ gradient (Buckhout, 1989; Bush, 1990;
67 Michonneau *et al.*, 2004).

68 With the beginning of the molecular era, the nature of the first plant glucose and sucrose
69 transporters were identified (Sauer & Tanner, 1989; Sauer *et al.*, 1990; Riesmeier *et al.*,
70 1992). In 2013, the genome of *Beta vulgaris* was sequenced (Dohm *et al.*, 2014), providing
71 molecular access to the transporter inventory of sugar beet. Among them, BvSUT1 was
72 demonstrated to represent a proton-driven transporter sucrose loader of the sugar beet phloem
73 in source leaves (Nieberl *et al.*, 2017), while the BvTST2.1 transporter was shown to be
74 responsible for vacuolar sucrose accumulation in the sugar beet taproots (Jung *et al.*, 2015). In
75 patch-clamp studies with vacuoles of BvTST2.1-overexpressing tobacco mesophyll cells, this
76 sucrose-specific transporter was characterized as a proton/sucrose antiporter, which couples
77 the import of sucrose into the vacuole with the export of protons (Jung *et al.*, 2015) Release of
78 vacuolar sucrose and glucose is mediated by sugar symporters of the BvSUT4/AtSUC4 and
79 BvIMP/AtERDL6 types (Schulz *et al.*, 2011; Schneider *et al.*, 2012; Klemens *et al.*, 2014;
80 Rodrigues, C. M. *et al.*, 2020).

81 Despite recent advances in *in vitro* culture and genetic transformation technologies
82 incorporated with classical sugar beet breeding programs, it takes about 4 - 5 years to generate
83 transgenic sugar beet plants. Low regeneration and transformation frequencies still oppose
84 serious restrictions for routine application of transformation technologies (Gurel *et al.*, 2008).
85 Thus, after almost 40 years of research our current knowledge about sugar transport in *Beta*

86 *vulgaris* is essentially that of the 1980's (Wyse, 1979; Saftner & Wyse, 1980; Saftner *et al.*,
87 1983; Lemoine *et al.*, 1988; Fieuw & Willenbrink, 1990) and is restricted to leaf phloem
88 loading and taproots' vacuolar transport. The molecular identity and the functional properties
89 of transporters that provide for sugar uptake into the taproot storage parenchyma cells is
90 unknown.
91 Plants respond to cold temperatures by accumulating compatible solutes (e.g., proline,
92 polyols, soluble sugars such as sucrose, glucose and fructose) to protect cellular integrity
93 (Wanner & Junttila, 1999; Gusta *et al.*, 2004; Krasensky & Jonak, 2012; Klemens *et al.*,
94 2014; Tarkowski & Van den Ende, 2015). Interestingly, altered vacuolar glucose levels are
95 accompanied by changes in vacuolar sugar transporter gene activities. In Arabidopsis plants, a
96 lower transcript level of the vacuolar glucose unloader AtERDL6 alongside a higher level of
97 the vacuolar glucose loader AtTST1/2 was detected upon cold exposure (Poschet *et al.*, 2011).
98 Further results from studies with AtTST1 loss-of-function and BvIMP-overexpressing
99 Arabidopsis plants suggested that the ability of the plant to accumulate monosaccharides in
100 vacuoles under cold conditions accounts for frost tolerance (Klemens *et al.*, 2014). In
101 comparison, in cold-treated sugar beet taproots, the transcription of the vacuolar sucrose
102 loader BvTST2.1, which is a homolog to AtTST1/2, was down-regulated, whereas that of the
103 vacuolar sucrose unloader BvSUT4 increased (Rodrigues, Cristina Martins *et al.*, 2020), a
104 finding that may be related to the cold sensitivity of the sugar beet plant.

105 To elucidate the nature of sucrose and glucose transport function in taproot of sugar beet, in
106 this study, we employed *in vivo* voltage-recording and proton-sensing microelectrodes to
107 monitor sucrose- and glucose-dependent changes in the membrane voltage and H^+ flux in
108 taproot slices directly. To identify the molecular players, we conducted comprehensive
109 phylogenetic and transcriptomic analysis of the sugar beet monosaccharide transporter (MST)
110 family proteins and sugar beet taproot tissue during low temperatures. We identified the
111 taproot expressed BvPMT5a and BvSTP13, both are up-regulated upon exposure to cold
112 temperatures. Thorough electrophysiological characterization using *Xenopus laevis* oocytes as
113 a functional expression system together with molecular modelling identified both carriers as
114 the long-sought proton-driven transporters sugar exhibiting distinct substrate specificities.
115 Based on these results, we conclude that both BvPMT5a and BvSTP13 are well suited to
116 mediate differential glucose and sucrose uptake across the taproot plasma membrane and
117 discuss their possible physiological role during sugar beet cold stress adaptation.

118

Materials and Methods

Plant material and cultivation

For electrophysiological characterization and RT-qPCR analysis, *Beta vulgaris* plants (GT1-3 hybrids, Lisanna) derived from KWS SAAT SE (Germany) were cultivated on Profi Substrat soil (CL ED73 Puls + Eisen, Einheitserde Werkverband e.V) under a 14/10 h day/night regime with a light intensity of about 120 µmol m^{-2} s^{-1} (sodium vapor lamp Sonte Agro 400) The temperature was 24 °C and the relative humidity 60%.

Membrane voltage recordings in sugar beet taproots

Plants of 95 to 115 days old were used for membrane voltage recordings. The taproots were harvested, and cross sections of whole root prepared (middle part of the root, 0.5 mm slice). From these slices, the periderm was detached with sharp forceps to create a window. The tissue in this window was cut tangential to get a sample of 10 to 15 cell layers thick. The sample was glued with medical adhesive B liquid (ULRICH Swiss, St Gallen, Switzerland) to a cover glass, which was mounted with double-sided adhesive tape in the lid of a 3 cm Petri dish. It was bathed in 3 mL measuring solution (1 mM $CaCl_2$, 1 mM KCl, 10 mM 2-(N-morpholino)ethanesulfonic acid (MES), adjusted with Bis-Tris propane (BTP) to pH 6.0) and the sample was incubated for 16 h at 18 °C in the dark. The solution was changed 1 h before measurement, and samples remained in the dark. The free-running membrane voltage recordings were essentially performed as described (Reyer *et al.*, 2020). Briefly, glass microelectrodes made of borosilicate glass capillaries (length 100 mm, $Ø_{outer}$ 1.0 mm, wall thickness 0.21 mm, Hilgenberg GmbH, Malsfeld, Germany) and filled with 300 mM KCl were impaled into the cells under microscopic control. The acquired data were analyzed using Microsoft Excel 2010 and Origin Pro-2021.

Proton flux measurements on sugar beet taproots

For application of the scanning ion-selective electrode (SISE) technique (Dindas *et al.*, 2018), taproots were cut into slices (Ø ~ approx. 0.5 cm) and an intact layer of parenchyma cells was dissected from a small area of such a slice. The entire slices were then immediately incubated in a basic salt medium (BSM, 0.5 mM KCl; 0.1 mM CaCl, pH 5.3 unbuffered) and left overnight in the dark at room temperature. One hour prior to measurement, the slices were mounted with non-woven microporous adhesive tape (URGOPORE, 1.25 cm, Urgo Medical, Chenôve, France) on Petri dishes (diameter 8.5 cm) and subsequently filled with 25 mL of

153 BSM. Thirty minutes prior to measurement, the BSM solutions in the petri dishes were
154 changed. Net H^+ fluxes were then measured from the exposed cells using non-invasive H^+-
155 selective scanning microelectrodes. According to (Newman, 2001) and (Dindas *et al.*, 2018),
156 microelectrodes were pulled from unfilamented borosilicate glass capillaries (Ø 1.0 mm,
157 Science Products GmbH, Hofheim, Germany) dried over night at 220 °C, then silanized with
158 N,N-dimethyltrimethylsilylamine (Sigma-Aldrich) for 1 h. The electrodes were subsequently
159 back-filled with a backfilling solution (15 mM NaCl/40 mM KH_2PO_4, pH adjusted to 6.0
160 using NaOH for H^+) and front-filled with an H^+-selective ionophore cocktail (catalogue
161 number 95291 for H^+, Sigma-Aldrich). Calibration of H^+-selective electrodes was performed
162 at pH 4.0, pH 7.0 and pH 9.0. Electrodes with slope > 50 mV per decade and correlation >
163 0.999 were used for measurements. After calibration, the electrode was placed at a distance
164 approximately 40 µM from the taproot sample using a SM-17 micromanipulator (Narishige
165 Scientific Instrument Lab) and an upright microscope (Axioskop; Carl Zeiss AG,
166 Oberkochen, Germany). During measurements electrodes were moved between two positions,
167 i.e., close to and away from the sample (40 µm and 140 µm, respectively) at 10 s intervals
168 using a micro-stepping motor driver (US Digital, Vancouver, WA, USA). The difference in
169 the potentials between these two points was recorded with a NI USB 6259 interface (National
170 Instruments), controlled by a custom-made, Labview-based software 'Ion Flux Monitor'. The
171 recorded potential was converted offline into proton flux values using the Labview-based
172 program 'Ion Flux Analyser', Excel 2010 and Origin Pro 2021 software.
173
174 **Current recordings from *Xenopus laevis* oocytes**
175 The two-electrode voltage-clamp technique was applied to *Xenopus laevis* oocytes injected
176 with complementary RNA coding for BvPMT5a and BvSTP13 essentially as described by
177 (Wittek *et al.*, 2017). A standard bath solution was used for the membrane current recordings:
178 100 mM KCl, 1 mM $CaCl_2$, 1 mM $MgCl_2$, 1 mM $LaCl_3$, adjusted to 220 mosmol kg^{-1} with D-
179 sorbitol or sucrose. Solutions were adjusted either to pH 5.5 with MES/Tris buffer or to pH
180 6.5 and pH 7.5 with HEPES/Tris buffer. The following sugar compounds were added to the
181 solutions at the concentrations indicated in the figure legends: L-(+)-arabinose, D-(–)-
182 fructose, L-(-)-fucose, D-(+)-galactose, D-(+)-glucose, glycerol, D-glucuronic acid, D-
183 mannitol, D-(+)-mannose, myo-inositol, D-(+)-raffinose, L-rhamnose, D-sorbitol, sucrose,
184 xylitol. Sugar-induced current responses were determined by subtracting the current responses
185 at the end of sugar application from those before sugar administration. For this, usually 150
186 ms lasting voltage pulses in the range of 0 to -140 mV were applied in 10-mV decrements

187 before and during sugar application, starting from a holding voltage of -40 mV. Current
188 responses to sugar application were also determined from continuous recordings at a constant
189 membrane voltage.
190 To study the temperature dependency of the sugar transporters in oocytes, the bath solution
191 passed through a heat exchanger in contact with peltier elements on which the recording
192 chamber was mounted. The temperature was measured with a small thermistor close to the
193 oocyte. In these experiments, the bath solution for BvPMT5-expressing oocytes contained 75
194 mM NaCl, 50 mM sucrose, 1 mM $CaCl_2$, 1 mM $MgCl_2$, 1 mM $LaCl_3$ and 10 mM MES/TRIS,
195 pH 4.5. To induce uptake currents, sucrose was replaced by 50 mM D-(+)-glucose. The bath
196 solution for BvSTP13-expressing oocytes contained 96 mM NaCl, 2 mM KCl, 1 mM $CaCl_2$, 1
197 mM $MgCl_2$, 1 mM $LaCl_3$, 0.5 mM D-sorbitol, and 10 mM Mes/Tris, pH 4.5. To induce uptake
198 currents, D-sorbitol was replaced by 0.5 mM D-(+)-glucose.
199 Data acquisition and offline analysis were performed using the software programs Patch
200 Master (HEKA Electronik, Lambrecht, Germany), Microsoft Excel, Origin2021 (OriginLab
201 Corporation, Northampton, MA 01060 USA) and IgorPro (Wave Metrics Inc., Lake Oswego,
202 OR, USA).
203
204 **Molecular cloning of sugar beet transporter**
205 To generate constructs for heterologous expression of fluorophore-labelled or untagged
206 *BvPMT5a* or *BvSTP13*, the corresponding coding sequence was amplified from cDNA of root
207 tissue from cold-treated sugar beets. PCR-amplification of target sequences using the primer
208 pNBI-BvPMT5-f (5'- GGG CTG AGG CTT AAT ATG AGT GAA GGA ACT AAT AAA
209 GCC ATG -3') together with BvPMT5-pNBI16/21-r (5'- ATT CGC TGA GGT TTA GTG
210 ATT GTC ATT TGT AAC AGT AGT ACT A -3'), or pNBI-BvSTP13-f (5'- ATT CGC TGA
211 GGT TTA GTG ATT GTC ATT TGT AAC AGT AGT ACT A -3') together with BvSTP13-
212 pNBI16/21-r (5'- ATT CGC TGA GGT TTA TAG AGC TGC AGC TGC AGC AGA CCC
213 ATT AT -3') yielded PCR-fragments for cloning into pNBI16 (no tag), or pNBI21 (N-
214 terminal fluorophore), respectively. PCR using the primer pairs pNBI-BvPMT5-f and
215 BvPMT5-pNBI22-r (5'- CCA GGC TGA GGT TTA AGT GAT TGT CAT TTG TAA CAG
216 TAG TAC TA -3'), or pNBI-BvHT2-f BvSTP13-pNBI22-r and BvSTP13-pNBI22-r (5'- CCA
217 GGC TGA GGT TTA ATA GAG CTG CAG CAG ACC CAT TAT -3'), removed the stop
218 codon of the transporter CDSs to allow generation of fusions to the N-terminus of the yellow
219 fluorescent Venus (pNBI22), respectively. PCR fragments were directly cloned into the *PacI*-
220 linearized expression vectors (pNBI16, pNBI21, or pNBI22) using the In-Fusion® HD

221 Cloning Kit (Takara Bio USA, Inc.). Insert sequences were verified by sequencing (Eurofins,
222 Germany).
223
224 **Phylogenetics of sugar transporters**
225 The phylogenetic relationships *Arabidopsis thaliana* and *Beta vulgaris* PMT and STP
226 transporters were studied by aligning the derived amino acid sequences using the MUSCLE
227 plugin (Edgar, 2004) within Geneious (Biomatters, Inc., San Diego, CA) with default
228 parameters. The alignments were trimmed using trimAl v1.2rev59 (Capella-Gutierrez *et al.*,
229 2009) using the implemented 'gappyout' algorithm. Phylogenetic reconstruction of the MSA
230 was conducted using IQ-TREE multicore version 2.1.2 (Minh *et al.*, 2020). The best-fit
231 substitution models were LG+G4 and LG+I+G4 for the PMT and STP datasets, respectively,
232 and were selected based on the Bayesian Information Criterion and implemented in the
233 Maximum Likelyhood (ML) tree reconstruction. Branch support was estimated using 1000
234 replicates and ultrafast bootstrap (Hoang *et al.*, 2018). Consensus trees were finally visualized
235 employing the iTol online tool (https://itol.embl.de/).
236
237 **3D modeling of BvSTP13 and molecular dynamic analysis of saccharide binding**
238 A 3D homology model of BvSTP13 was obtained based on the crystal structure of
239 *Arabidopsis thaliana* STP10 (PDB entry 6H7D; Paulsen *et al.*, 2019) using the modeling
240 macro hm_build.mcr of the software package YASARA Structure version 20.12.24
241 (https://www.yasara.org, Krieger and Vriend, 2014; PMID 24996895). Briefly, the amino acid
242 sequence of BvSTP13 covering residues Met1 to Leu537 was aligned to the sequence of
243 STP10 using a PSI-BLAST search against the RCSB databank with a maximum E-value of
244 0.1 for template consideration. Three potential templates were identified: PDB entries 6H7D
245 (AtSTP10, Paulsen *et al.*, 2019), 4ZW9 (HsGTR3, Deng *et al.*, 2015) and 5C65
246 (HsGTR3/SLC2A3; Pike A.C.W. *et al.* unpublished), although the latter two exhibited
247 considerably lower scores in YASARA's PSI-Blast search and alignment. For modeling a
248 secondary structure prediction, a target sequence profile was built against related UniRef90
249 sequences. Fourteen initial homology models were then built using the template AtSTP10
250 (PDB entry 6H7D), employing five slightly different sequence alignments that differed in the
251 adjustments of loop regions. Of these, two exhibited the best overall Z-scores of -0.432
252 and -0.465 in the YASARA scoring routine after energy minimization and molecular
253 dynamics refinement. The model used for analysis comprised 505 amino acid residues
254 harboring Gly12 to Ala516, the 11 N-terminal and the 21 C-terminal amino acids were not

255 modeled because there is no template structure available for these residues. However, from
256 the model it can be assumed that these residues are flexible and adopt a dynamic structure.
257 The final model also contained the glucose moiety present in the original template AtSTP10
258 (PDB entry 6H7D), which engaged in an identical hydrogen bond pattern with surrounding
259 residues in BvSTP13. This was because all amino acids in close proximity to the glucose
260 moiety are conserved between AtSTP10 and BvSTP13. To obtain further insights into
261 possible saccharide binding and specificity of BvSTP13, the monosaccharide fructose and the
262 disaccharide sucrose were also docked in the saccharide binding site of the model. A short
263 molecular dynamic simulation of the BvSTP13 model placed in a membrane layer with either
264 bound glucose, fructose or sucrose was run using YASARA's macro md_runmembrane.mcr.
265 The hexaoxaicosandiol/PEG moiety that was part of the crystallization solution/condition of
266 the original AtSTP10 crystal and which artificially occupied part of the inner binding cleft
267 partially filled with the glucose molecule was removed before the MD simulation. The
268 membrane region of the BvSTP13 molecule was predicted by YASARA. The BvSTP13
269 model was then centered in a box with the dimensions 83 x 83 x 113 Å and with the
270 membrane region of the BvSTP13 model placed in the lipid bilayer comprising 159
271 phosphatidyl-ethanolamine molecules. Water was put above and below the membrane bilayer,
272 sodium and chloride ions were placed at a concentration of 150 mM and to neutralize the
273 protein charges within the box. After energy minimization of the membrane bilayer, the water
274 solvent molecules and ions, an unrestrained molecular dynamic simulation was performed at
275 298K (25 °C) and constant pressure for 5 (BvSTP13 with glucose bound) and 10 ns
276 (BvSTP13 with sucrose or fructose bound). The MD trajectories were analyzed with
277 YASARA with respect to hydrogen bonding between the saccharide molecules and the sugar
278 transporter.
279
280
281
282 # Results
283 **Sugar uptake in taproots is directly linked to proton influx and membrane**
284 **depolarization**
285 As soon as sucrose is translocated from the source leaves to the taproot and released from the
286 phloem to the apoplast, sucrose needs to enter the storage parenchyma cells (Lemoine *et al.*,
287 1988; Godt & Roitsch, 2006). For this, sucrose is most likely translocated across the plasma
288 membrane via H^+-coupled sugar uploaders. To date, insights into *Beta vulgaris* taproot sugar

289 transport have mostly been gained by classical physiological assays such as uptake of
290 radioactive sugars into tissue slices (*in vivo*) and plasma membrane enriched vesicles (*in*
291 *vitro*). Based on the ground-breaking findings on *Beta vulgaris* sugar transport gained with
292 taproot slices, we took advantage of the same experimental system. To first visualize cellular
293 sucrose loading in the storage organ, we employed the fluorescent sucrose analog esculin,
294 which is accepted by several sucrose transporters as a substrate for membrane translocation
295 (Gora *et al.*, 2012; Reinders *et al.*, 2012; Abelenda *et al.*, 2019). After prolonged incubation
296 of taproot slices from maturating 14 to 18-week-old sugar beets with esculin for 90 or 180
297 minutes (Method S1), a strong fluorescent signal was detected around the nucleus (Fig. S1a).
298 This indicates the uptake of esculin from the apoplast into the cytosol of parenchyma cells.
299 The results with this fluorescent ß-glycoside suggest that sucrose transporters are present in
300 the plasma membrane and are capable of shuttling sucrose into the cytosol.
301 Given that a secondary active rather than a passive transport for apoplastic high-capacity
302 sugar loading of the taproot parenchyma cells is the most likely mechanism, we next
303 investigated the plasma membrane electrical phenomena underlying sucrose and glucose
304 uptake using voltage-recording and ion-selective electrodes. For online recording of sucrose-
305 and glucose-induced changes in H^+ fluxes across the plasma membrane of taproot cells non-
306 invasively, we employed scanning H^+-selective electrodes (cf. Reyer *et al.*, 2020). In taproot
307 slices from 14 to 16-week-old maturating sugar beets, resting parenchyma cells were
308 characterized by H^+ efflux activity, as is expected from the plasma membrane H^+ pump (Fig.
309 1a). In line with a proton-coupled sugar symporter, administration of both glucose and
310 sucrose (50 mM) resulted in a decreased H^+ efflux for often at least 30 minutes (Fig. 1a, Fig.
311 S2a). During this glucose and sucrose evoked phase, maximum proton fluxes of 25.8 ± 7.2
312 nmol m^{-2} s^{-1} (n = 11, SEM) and 24.1 ± 7.4 nmol m^{-2} s^{-1} (n = 11, SEM) respectively, were
313 measured. This response indicated that the plasma membrane of the parenchyma cells from
314 slices derived from sugar-accumulating taproots is sucrose and glucose transport competent.
315 In plant cells, the plasma-membrane proton efflux results from the H^+ pump activity of
316 vanadate sensitive AHA-type H^+-ATPases (cf. Reyer *et al.*, 2020, and references therein).
317 Since sugars are not charged while protons are, one must predict that the phenomenon
318 observed for the H^+ fluxes (Fig. 1a, Fig. S2a) is best explained mechanistically by H^+/sugar
319 co-import. To monitor sugar-induced membrane potential changes, cells of the afore
320 identified sugar-sensitive taproot slices were impaled with voltage recording microelectrodes.
321 The membrane potential was -149.9 ± 3.3 mV (n = 18, SEM) at rest, and transiently
322 depolarized by 48.3 ± 6.1 mV (n = 7, SEM) and 51.6 ± 3.7 mV (n = 6, SEM) upon addition of

323 50 mM glucose and sucrose, respectively (Fig. 1b, Fig. S2b). Without removal of sugar, the
324 membrane voltage generally slowly relaxed to the pre-stimulus level; a behavior in line with a
325 depolarization and H^+ influx-dependent activation of the H^+-ATPase (Reyer *et al.*, 2020).
326 Taken together, our electrophysiological studies with taproot slices indicate that sugar-
327 accumulating taproot cells are equipped with a proton-pumping moiety that drives H^+-coupled
328 sucrose and glucose transport. These findings raise questions about the molecular nature and
329 sugar specificity of the transporters involved.
330
331 **Low temperatures stimulate *BvPMT5a* and *BvSTP13* transporter expression in taproots**
332 Possible candidates for mediating the observed sugar/H^+ fluxes across the plasma membrane
333 are likely found among members of the Monosaccharide Transporter (MST) superfamily
334 (Büttner, 2007; Pommerrenig *et al.*, 2018). Of the seven MST subfamilies, only the INT, STP
335 and PMT subfamilies harbor plasma membrane transporters (Scholz-Starke *et al.*, 2003;
336 Klepek *et al.*, 2005; Schneider *et al.*, 2006; Schneider *et al.*, 2007; Klepek *et al.*, 2010;
337 Rottmann *et al.*, 2018). INT subfamily members have been reported as carriers for inositol
338 and other polyols, but not for sucrose (Schneider *et al.*, 2006; Schneider *et al.*, 2007). In
339 contrast, STPs and PMTs exhibit a high specificity for the monosaccharides glucose and
340 fructose (Klepek et al., 2005; Rottman et al., 2018). Astonishingly, the MdSTP13a homolog
341 from apple (*Malus domesticus*) has recently been shown to transport the disaccharide sucrose,
342 in addition to the monosaccharide glucose (Li *et al.*, 2020). In our further sugar beet studies,
343 we therefore concentrated on STPs and PMTs. The *Beta vulgaris* genome encodes 14 putative
344 STP-type transport proteins and five PMTs (Fig. S3). Among these, BvSTP13 and BvPMT5a
345 are of particular interest because their mRNA levels were markedly increased in taproots
346 upon exposure to low temperatures (Fig. S4, Method S2). These data suggest a possible role
347 for these two transporters in the taproot tissue of sugar beet during the cold stress response.
348
349 **BvPMT5a is a proton-coupled glucose and polyol transporter**
350 To gain insights into the possible role of BtPMT5a in taproot sugar uptake and in relation to
351 the electrophysiological *in vivo* recordings from the taproot slices (Fig. 1, Fig. S2), the
352 transport features of BvPMT5a were analyzed in *Xenopus laevis* oocytes via voltage-clamp
353 recordings (Carpaneto *et al.*, 2005; Nieberl *et al.*, 2017). When BvPMT5a-expressing oocytes
354 were exposed to the disaccharide sucrose (10 mM) at pH 5.5 and a membrane voltage of -40
355 mV, no additional current to the current background noise was elicited. However, application
356 of glucose or fructose caused similar pronounced inward currents (Fig. 2a, b). In addition to

357 the monosaccharides released by sucrose breakdown via invertase activity, BvPMT5a-
358 expressing oocytes were challenged with the glucose derivative glucuronic acid, hexose
359 deoxy sugars fucose and rhamnose, pentose arabinose, and various polyols (sorbitol,
360 mannitol, myo-inositol, glycerol, xylitol). Among these, mannitol, glucuronic acid and
361 glycerol only produced very weak inward currents. Sorbitol, arabinose, fucose, rhamnose and
362 myo-inositol induced similar currents to glucose and fructose, while xylitol caused the largest
363 current response (Fig. 2b). This behavior of BvPMT5a points to a transporter of broad
364 substrate specificity. Due to the favorable signal-to-background-noise ratio with xylitol as a
365 BvPMT5a substrate, this polyol was selected as a representative substrate to study the
366 involvement of protons as a potential co-substrate in the translocation process. As expected
367 from a H^+-driven monosaccharide/polyol transporter, in the presence of 10 mM xylitol
368 polyol-induced inward currents became smaller when at a membrane voltage of -40 mV, the
369 external pH was increased, and the proton motive force (PMF) was decreased in steps from
370 5.5 to 6.5 and 7.5 (Fig. S5a). At a membrane voltage of 0 mV and pH of 7.5, a value where
371 the extracellular and cytosolic proton concentrations match, the PMF is zero (Fig. S5b).
372 Nevertheless, polyol application still elicited inward currents that reached about 25% of those
373 driven by a 100-fold H^+ gradient at pH 5.5 (Fig. S5b). In the absence of a PMF, H^+ uptake
374 into the cell was driven solely by the polyol concentration gradient directed into the cytosol.
375 When the membrane voltage became increasingly hyperpolarized, the PMF increased,
376 resulting in larger inward currents under any pH situation. However, at voltages more
377 negative than -80 mV, the xylitol-induced currents measured at pH 6.5 and 5.5 became very
378 similar, suggesting that the maximal transport capacity reached a similar level under both pH
379 conditions and is no longer promoted by the voltage part of the PMF. When instead of the
380 external pH, the xylitol concentration was varied by adding either 1, 3, 5, 10, 20, 30, 50 or
381 100 mM xylitol, the inward current increased stepwise from a concentration of 1 to 20 mM,
382 saturating above 30 mM (Fig. 3a,b). This saturation behavior could be fitted with a Michaelis-
383 Menten function from which a K_m value of 2.5 mM was derived (Fig. 3b,c). When the
384 electrical driving force was increased from -40 to -140 mV, reflecting the resting membrane
385 voltage of the taproot parenchyma cells (Fig. 1b, Fig. S2b), the affinity to this polyol substrate
386 increased almost two-fold as the K_m dropped from 2.5 to 1.5 mM (Fig. 3c). In analogous
387 experiments involving the glucose-dose dependency of BvPMT5a (Fig. 3d-f), the derived K_m
388 values for glucose also decreased (Fig. 3e,f), indicating that the PMF is energizing the
389 BvPMT5a H^+/glucose cotransport. This identifies BvPMT5a as a potential candidate for
390 glucose uploading in beet roots.

391

392 **BvSTP13 operates as a high-affinity, proton-coupled glucose and sucrose transporter**

393 Like BvPMT5a, BvSTP13 was heterologously expressed and its transport features
394 characterized in *Xenopus laevis* oocytes. At an external pH of 5.5 and a membrane potential
395 of -40 mV, BvSTP13-expressing oocytes were exposed to various monosaccharides as well as
396 to di- and trisaccharides (Fig. 4a). Upon application of 10 mM hexose quantities, BvSTP13-
397 mediated inward currents of similar large amplitudes were recorded with glucose, fructose,
398 galactose and mannose. In contrast, the polyols sorbitol, myo-inositol and xylitol, the hexoses
399 rhamnose and fucose, the pentose arabinose and the hexose derivative glucuronic acid all
400 caused no or only small currents. The aldopentose xylose, however, triggered current
401 responses that reached approximately 70% of those obtained with glucose. When exposed to
402 the glucose-fructose disaccharide sucrose, similar pronounced inward currents to those with
403 xylose were obtained. Unexpectedly, even the trisaccharide raffinose evoked current
404 responses of amplitudes that were still about 40% of those reached with glucose. BvSTP13
405 also accepted the sucrose surrogate esculin as a substrate (Fig. S6a). These current responses
406 demonstrate that BvSTP13 is not a typical hexose transporter; it is capable of transporting not
407 only certain monosaccharides but also sucrose and raffinose.

408 To determine the glucose-dose dependency of the BvSTP13 transporter, the glucose
409 concentration was increased stepwise from 0.05 mM to 1.0 mM (Fig. 4b). In these
410 experiments, inward currents were evoked with as little as 0.05 mM glucose. Currents tended
411 to saturate when the substrate concentration was raised above 0.1 mM (Fig. 4b,c). The K_m
412 value at a membrane potential of -40 mV for glucose was 0.075 mM (Fig. 4c,d), indicating
413 that BvSTP13 represents a high-affinity sugar transporter. Like glucose, the application of
414 sucrose elicited H^+ inward currents at a concentration as low as 0.05 mM (Fig. 6a,b),
415 suggesting that BvSTP13 also has a high affinity to sucrose. At the glucose and sucrose
416 concentrations tested, membrane hyperpolarization and an acidic external pH enhanced the
417 inward currents (Fig. 4e, Fig. S6b,c, Fig. S7). Together, the voltage and pH dependency of the
418 BvSTP13-mediated currents demonstrate that as with BvPMT5a, the BvSTP13-mediated
419 sugar translocation is proton-coupled, so thermodynamically driven by the proton motive
420 force and the sugar gradient (cf. Carpaneto *et al.*, 2005; Reinders *et al.*, 2005; Wittek *et al.*,
421 2017). However, in contrast to BvPMT5a (Fig. 3f), the K_m values of BvSTP13 for glucose
422 surprisingly increased to about 0.16 mM upon hyperpolarization to -140 mV. This indicates
423 that BvPMT5a gains a higher sugar affinity when the membrane potential is depolarized.

424 BvPMT5a and BvSTP13 were noticed because they become transcriptionally up-regulated
425 upon exposure to low temperatures (Fig. S4). Thus, in addition to parameters such as the PMF
426 and voltage dependence, we asked how carrier function and thermodynamics respond to
427 temperature changes. In the Xenopus oocyte system, the temperature was lowered from 35 to
428 5 °C in 10 °C steps, and the glucose-induced current responses were monitored (Fig. 5).
429 Current amplitudes with both transporters decreased with each cooling step. However,
430 BvPMT5a-mediated currents could only be resolved when the temperature was raised above
431 5 °C. Above this temperature threshold, warming up the oocyte by 10 °C steps increased the
432 transporter activity with a Q_{10} of about 4. In contrast, significant BvSTP13-related currents
433 were recorded already at 5 °C and were characterized by a Q_{10} of about 2.
434
435 **Modeling the BvSTP13 structure with bound mono- and disaccharide**
436 To obtain the first insights into the molecular nature of the broad sugar specificity of
437 BvSTP13, we modeled BvSTP13, based on the known structure of the monosaccharide
438 transporter AtSTP10 from *Arabidopsis thaliana* (Rottmann *et al.*, 2016; Paulsen *et al.*, 2019;
439 Bavnhøj *et al.*, 2021). In accordance with their shared overall 6TM-loop-6TM topology (TM,
440 transmembrane domain), the BvSTP13 amino acid sequence could be perfectly mapped onto
441 the AtSTP10 structure (Fig. S8). The 3D model obtained for BvSTP13 revealed all the
442 structural hallmarks of the STP protein family. This includes the existence of a characteristic
443 'lid-domain' covering the extracellular entry pathway to the sugar binding site, and a cavity
444 that is formed between the N-terminal and C-terminal halves of the sugar transporter (Fig.
445 S8a). The structural alignment further revealed that core amino acid residues, identified as
446 constituting the binding sites for coordinating the glucose substrate (Paulsen *et al.*, 2019),
447 were perfectly conserved between both transporters, with the exception of Leu43 in AtSTP10,
448 which is replaced conservatively by valine (Val44) in BvSTP13 (Fig. S8b). The presence of a
449 hydrophilic polyethylene glycol (PEG) moiety above the bound glucose molecule in the
450 AtSTP10 structure and resulting (artificially) from the crystallization conditions indicates that
451 the saccharide binding cleft in the determined outward open conformation is wide enough to
452 accommodate carbohydrates larger than monosaccharides (Fig. 6). In our model of BvSTP13
453 bound with sucrose, space for the second carbohydrate moiety of the disaccharide is provided
454 by changes in the sidechain conformation of Asn304 and Met307. This suggests that the
455 spatial requirements of sucrose accommodation could seemingly be fulfilled in BvSTP13 as
456 well as in AtSTP10. A molecular dynamics (MD) simulation of our BvSTP13 model placed
457 in an explicit solvent/membrane bilayer and having either a glucose or sucrose molecule

458 bound did not provide hints as to why BvSTP13 should exhibit stringent specificity for
459 binding either glucose or sucrose (Fig. 6).
460 The proton donor/acceptor residue pair needed for proton translocation, Asp42 and Arg142 in
461 AtSTP10, is preserved in BvSTP13 as well as in the polyol transporter BvPMT5a. However,
462 amino acid residues involved in substrate coordination partially differ between polyol and
463 sugar transporters. Markedly, BvPMT5a lacks a 'lid domain' (Fig. S9). Specific for members
464 of the STP family, this 'lid domain' connects the N- and C-terminal moieties of the
465 transporter via a disulfide bridge. Recent work by Bavnhøj et. al (2021) shows that following
466 sugar binding and protonation of the Asp42 the 'lid domain' undergoes dramatic structural
467 rearrangements and isolates the protonation site from the apoplast to define an outward
468 occluded state. During transition to an inward open state the 'lid domain' moves again and –
469 via the conserved disulfide bond - locks the central helices of the N- and C-terminal
470 transmembrane domains together, isolating both the protonation and the sugar biding site
471 binding site from the extracellular space. Our modeling approach revealed that the 'lid
472 domain' differs between AtSTP10 and BvSTP13, in particular, the non-structured loop C-
473 terminal to the two short helices in the apoplastic loop between TM1 and TM2 (Fig. S8a).
474
475
476
477 ## Discussion
478 **BvPMT5a and BvSTP13 together function as low and high-affinity proton-driven**
479 **glucose importers**
480 To discover the solute moiety transported by the phloem *in vivo*, aphid stylectomy was used
481 to identify sucrose as the major sugar (Fisher *et al.*, 1992). Furthermore, aphid stylectomy in
482 combination with electrophysiology revealed that sucrose-uptake into the phloem depolarizes
483 the membrane potential of the sieve elements (Carpaneto *et al.*, 2005). Sucrose in the plant is
484 disseminated from source to sink via the phloem network. In sink organs such as a taproot in
485 the case of sugar beet, sucrose exits the phloem apoplastically (Lemoine *et al.*, 1988; Godt &
486 Roitsch, 2006). However, depending on the activity of extracellular invertase at the exit site
487 (Lemoine *et al.*, 1988; Jammer *et al.*, 2020), parenchyma sugar transporters will be faced with
488 glucose and fructose in addition to sucrose. Our electrophysiological studies with taproot
489 parenchyma cells clearly demonstrate that the plasma membrane responds to glucose and
490 sucrose, as expected from transporter-mediated proton-driven sugar import (Fig. 1, Fig. S2).
491 Two cold-associated transporters BvPMT5a and BvSTP13 were characterized in the oocyte

492 system as H^+/solute symporters (Figs 2-5, Figs S5-7). BvPMT5a mediates the proton-coupled
493 import of glucose with a millimolar affinity (Fig. 3). BvSTP13 shuttles both glucose and
494 sucrose with submillimolar affinities (Fig. 4, Fig. S6a,b), probably similar to AtSTP1 with a
495 1:1 stoichiometry in cotransport with a proton (Boorer *et al.*, 1994). Thus together, BvPMT5a
496 and BvSTP13 provide for high and low-affinity glucose uptake (Figs 3f, 4d). Whether the
497 opposite weak voltage dependency of the BvSTP13 glucose affinity is correlated with a
498 spatial rearrangement of substrate binding sites during the transport cycle conferred by the
499 'Lid domain' – present in BvSTP13 but absent in BvPMT5a (Fig. S9) – needs to be explored
500 in further studies. That (i) taproot parenchyma cells import esculin, (ii) according to MD
501 simulations, BvSTP13 is capable of binding glucose, sucrose and esculin, and (iii) in
502 electrophysiological experiments, BvSTP13, like the apple MdSTP13a in radioactive tracer
503 experiments (Li *et al.*, 2020), was demonstrated to transport not only glucose and fructose but
504 also sucrose and esculin, suggests that this symporter is involved in the loading of
505 monosaccharides and possibly sucrose as well, into storage parenchyma cells.
506
507 **How to fit glucose and sucrose in the same transporter?**
508 The crystal structure of a member of the monosaccharide transporter superfamily, AtSTP10
509 with glucose bound, provided molecular insights into the hexose uptake mechanism (Paulsen
510 *et al.*, 2019). In contrast to the PMTs, a lid domain, which is conserved in all STPs, shields
511 both the sugar binding site and the proton binding site from the extracellular lumen. We used
512 homology models for BvSTP13 and MdSTP13a (Li *et al.*, 2020) and in silico docking of
513 various saccharides to unravel how possible differences in saccharide binding in different
514 members of the STP sugar transporter family might explain their observed substrate
515 specificity (Fig. 6, Fig. S8). In line with their similar saccharide specificity, all amino acid
516 residues in the binding cleft of the STP13 sugar transporter from sugar beet and apple (Li *et*
517 *al.*, 2020) were conserved within an 8 Å sphere of the glucose moiety position as found in
518 AtSTP10. Likewise, in this region only three amino acids differ between AtSTP10 and
519 BvSTP13, all other residues are identical (see also Fig. S8b). Based on the presence of three
520 water molecules and a hydrophilic polyethylene glycol molecule in the binding cleft just
521 above the glucose moiety, our MD simulations suggest that the binding site exhibits plasticity.
522 This binding cleft plasticity could allow to accommodate di- and trisaccharides in BvSTP13
523 (and possibly AtSTP10). The three amino acids, that differ between AtSTP10 and BvSTP13
524 are located below a conserved tryptophan (Trp410 and Trp412 in AtSTP10 and BvSTP13,
525 respectively). This residue resides beneath the saccharide binding cleft occupied by glucose

526 and can be considered a kind of dead-end of the sugar accommodating cavity. In the
527 structurally determined outward-open conformation (Paulsen *et al.*, 2019), the bulky indole
528 ring of Trp410 in AtSTP10 prevents further downward movement of the glucose towards the
529 transporters' cytoplasmic face. Because information on other required structural transporter
530 conformations is currently not available and that there is an apparent lack of difference in the
531 sugar binding, we cannot predict how these different residues affect saccharide binding or
532 transport specificity. Thus, the currently available structure (of only the outward open
533 conformation) (Paulsen *et al.*, 2019) can only provide insights into the binding situation when
534 the saccharide moiety enters the cleft and is coordinated at the glucose binding site. Neither
535 data for the transfer of the saccharide past the lid domain to the binding site nor for structural
536 changes in the transport protein accompanying their further translocation from the binding
537 cleft to the cytoplasmic site are available. The available structurally resolved conformations
538 of the Arabidopsis STP10 transporter together with molecular modelling and MD simulations
539 provides for testable predictions towards key residues determining sugar coordination and
540 substrate specificity during the transport cycle. Future work based on mutagenesis and
541 structure-function studies needs to elucidate whether the carbohydrate specificity of STP
542 transporters is determined by the binding site itself or is attributable to conformational
543 changes during their predicted outward open to inward open transport cycle.
544
545 **BvPMT5a and BvSTP13 with a possible role in cold response**
546 As with the plasma membrane sugar transporters BvPMT5a and BvSTP13, the expression of
547 the vacuolar Arabidopsis TONOPLAST SUGAR TRANSPORTERS TST1 and TST2 are
548 induced by low temperatures (Wormit *et al.*, 2006). During cold acclimation, *tst1/2* knockout
549 lines exhibited elevated sucrose levels, but reduced glucose and fructose levels in the leaves
550 compared with wild-type plants. This affected cold tolerance (Wormit *et al.*, 2006; Klemens
551 *et al.*, 2014); the cellular sugar content contributes to cold hardening. Together with their
552 transcriptional induction by cold, these observations suggest that for cold tolerance of the
553 sugar beet taproot, BvSTP13- and BvPMT5a-mediated plasma membrane hexose transport
554 may be important. In addition to sugars, polyols are also cold protective in nature, and these
555 are also substrates of BvPMT5a. Therefore, BvPMT5a and BvSTP13 together could provide
556 root parenchyma cells with cold protective compounds. Further studies will have to answer
557 this question. Functional expression of BvPMT5a and BvSTP13 in e.g. *Arabidopsis* wild type
558 and loss-of-sugar-transport-function mutants of the PMT5 and STP13 sub-clades (see Fig. S2)
559 will allow to study their impact on cold stress induced changes in plant/cell sugar levels and

profiles as well as their overall contribution to freezing tolerance (Jung et al. (2015), Wang et al. (2020) Nieberl et al. (2017) and Ho et al. (2019)).

In summary, our manuscript provides a gain in knowledge regarding the molecular identification of prime sugar transporter candidates of tap root cells. Our functional studies underline that these two transporters are strong candidates for the two different classes of monosaccharide transporters in *Beta vulgaris*. Additionally, we identified that BvSTP13 is also capable of transporting sucrose as a disaccharide as well as transporting monosaccharides. This astonishing finding could be underlined *in silico* by structure modelling bound with substrate. This model provides us a testable hypothesis for the molecular mechanism of the transport of glucose and sucrose by a member from a monosaccharide transporter family. Given that the temperature activity profiles of the two sugar transporters overlap, with BvSTP13 being more cold-resistant than BvPMT5a, it is tempting to speculate that during cold acclimation, these H^+ symporters work hand in hand.

Acknowledgements

This work was funded by a research grant to R.H. and H.E.N. by the Federal Ministry of Education and Research (project 'Betahiemis', FKZ 031B0185) and a King Saud University to R.H., K.A.S.A., A.H.A. and S.A.A. (Project ICSTD-2020/2). W.K. and F.L. are employees of KWS SAAT SE (Einbeck, Germany) and K.H. is an employee of Südzucker AG (Obrigheim/Pfalz, Germany). We thank Fábio Luiz Rogé Ferreira for his help in collecting raw electrophysiological data in Xenopus oocytes and Christina Müdsam for cloning of the sugar beet transporters.

Author Contributions

R.H., I.M., H.E.N., K.H., W.K., F.L. designed the research; A.R., J.J., N.B., N.S., S.S. performed research; A.R., D.J., J.J., N.B., N.S., T.D.M., D.B., S.S. analyzed data and R.H., I.M, D.B., T.D.M., K.A.S.A.-R., A.H.A., S.A.A., A.R., T.A.C., B.P., H.E.N. wrote the paper.

Data Availability

The data that support the electrophysiological/phylogenetic/structural findings and the RNA analysis of this study are available upon request from the corresponding author and Benjamin Pommerrening, respectively. RNA-seq data are found in the GenBank Sequence Read Archive (BioProject PRJNA602804).

Funding

This work was funded by a research grant to R.H. and H.E.N. by the Federal Ministry of Education and Research (project 'Betahiemis', FKZ 031B0185) and a King Saud University to R.H., K.A.S.A., A.H.A. and S.A.A. (Project ICSTD-2020/2). W.K. and F.L. are employees of KWS SAAT SE (Einbeck, Germany) and K.H. is an employee of Südzucker AG (Obrigheim/Pfalz, Germany).

Conflict of interest statement. None declared.

REFERENCES

Abelenda JA, Bergonzi S, Oortwijn M, Sonnewald S, Du M, Visser RGF, Sonnewald U, Bachem CWB. 2019. Source-Sink Regulation Is Mediated by Interaction of an FT Homolog with a SWEET Protein in Potato. *Curr Biol* **29**(7): 1178-1186 e1176.

Bavnhøj L, Paulsen PA, Flores-Canales JC, Schiøtt B, Pedersen BP. 2021. Molecular mechanism of sugar transport in plants unveiled by structures of glucose/H^+ symporter STP10. *Nature Plants*.

Boorer KJ, Loo DD, Wright EM. 1994. Steady-state and presteady-state kinetics of the H^+/hexose cotransporter (STP1) from Arabidopsis thaliana expressed in Xenopus oocytes. *J Biol Chem* **269**(32): 20417-20424.

Buckhout TJ. 1989. Surcose transport in isolated plasma-membrane vesicles from sugar beet (Beta vulgaris L.) Evidence for an electrogenic sucrose-proton symport. *Planta* **178**(3): 393-399.

Bush DR. 1989. Proton-Coupled Sucrose Transport in Plasmalemma Vesicles Isolated from Sugar Beet (*Beta vulgaris* L. cv Great Western) Leaves. *Plant Physiol* **89**(4): 1318-1323.

Bush DR. 1990. Electrogenicity, pH-Dependence, and Stoichiometry of the Proton-Sucrose Symport. *Plant Physiol* **93**(4): 1590-1596.

Büttner M. 2007. The monosaccharide transporter (-like) gene family in Arabidopsis. *FEBS Letters* **581**(12): 2318-2324.

Capella-Gutierrez S, Silla-Martinez JM, Gabaldon T. 2009. trimAl: a tool for automated alignment trimming in large-scale phylogenetic analyses. *Bioinformatics* **25**(15): 1972-1973.

Carpaneto A, Geiger D, Bamberg E, Sauer N, Fromm J, Hedrich R. 2005. Phloem-localized, proton-coupled sucrose carrier ZmSUT1 mediates sucrose efflux under the control of the sucrose gradient and the proton motive force. *J Biol Chem* **280**(22): 21437-21443.

637 **Deng D, Sun P, Yan C, Ke M, Jiang X, Xiong L, Ren W, Hirata K, Yamamoto M, Fan S,**
638 **et al. 2015.** Molecular basis of ligand recognition and transport by glucose
639 transporters. *Nature* **526**(7573): 391-396.
640 **Dindas J, Scherzer S, Roelfsema MRG, von Meyer K, Muller HM, Al-Rasheid KAS,**
641 **Palme K, Dietrich P, Becker D, Bennett MJ, et al. 2018.** AUX1-mediated root hair
642 auxin influx governs $SCF^{TIR1/AFB}$-type Ca^{2+} signaling. *Nat Commun* **9**(1): 1174.
643 **Dohm JC, Minoche AE, Holtgrawe D, Capella-Gutierrez S, Zakrzewski F, Tafer H,**
644 **Rupp O, Sorensen TR, Stracke R, Reinhardt R, et al. 2014.** The genome of the
645 recently domesticated crop plant sugar beet (*Beta vulgaris*). *Nature* **505**(7484): 546-
646 549.
647 **Edgar RC. 2004.** MUSCLE: multiple sequence alignment with high accuracy and high
648 throughput. *Nucleic Acids Res* **32**(5): 1792-1797.
649 **Fieuw S, Willenbrink J. 1990.** Sugar transport and sugar-metabolizing enzymes in sugar
650 beet storage roots (*Beta vulgaris* ssp. altissima). *Journal of Plant Physiology* **137**(2):
651 216-223.
652 **Fisher DB, Wu Y, Ku MS. 1992.** Turnover of soluble proteins in the wheat sieve tube. *Plant*
653 *Physiol* **100**(3): 1433-1441.
654 **Godt D, Roitsch T. 2006.** The developmental and organ specific expression of sucrose
655 cleaving enzymes in sugar beet suggests a transition between apoplasmic and
656 symplasmic phloem unloading in the tap roots. *Plant Physiol Biochem* **44**(11-12): 656-
657 665.
658 **Gora PJ, Reinders A, Ward JM. 2012.** A novel fluorescent assay for sucrose transporters.
659 *Plant methods* **8**: 13-13.
660 **Gurel E, Gurel S, Lemaux PG. 2008.** Biotechnology Applications for Sugar Beet. *Critical*
661 *Reviews in Plant Sciences* **27**(2): 108-140.
662 **Gusta LV, Wisniewski M, Nesbitt NT, Gusta ML. 2004.** The effect of water, sugars, and
663 proteins on the pattern of ice nucleation and propagation in acclimated and
664 nonacclimated canola leaves. *Plant Physiol* **135**(3): 1642-1653.
665 **Ho L-H, Klemens PAW, Neuhaus HE, Ko H-Y, Hsieh S-Y, Guo W-J. 2019.** SlSWEET1a
666 is involved in glucose import to young leaves in tomato plants. *Journal of*
667 *Experimental Botany* **70**(12): 3241-3254.
668 **Hoang DT, Chernomor O, von Haeseler A, Minh BQ, Vinh LS. 2018.** UFBoot2:
669 Improving the Ultrafast Bootstrap Approximation. *Mol Biol Evol* **35**(2): 518-522.
670 **Jammer A, Albacete A, Schulz B, Koch W, Weltmeier F, van der Graaff E, Pfeifhofer**
671 **HW, Roitsch TG. 2020.** Early-stage sugar beet taproot development is characterized
672 by three distinct physiological phases. *Plant Direct* **4**(7): e00221.
673 **Jung B, Ludewig F, Schulz A, Meißner G, Wöstefeld N, Flügge U-I, Pommerrenig B,**
674 **Wirsching P, Sauer N, Koch W, et al. 2015.** Identification of the transporter
675 responsible for sucrose accumulation in sugar beet taproots. *Nature Plants* **1**(1):
676 14001.
677 **Klemens PA, Patzke K, Trentmann O, Poschet G, Buttner M, Schulz A, Marten I,**
678 **Hedrich R, Neuhaus HE. 2014.** Overexpression of a proton-coupled vacuolar
679 glucose exporter impairs freezing tolerance and seed germination. *New Phytol* **202**(1):
680 188-197.
681 **Klepek YS, Geiger D, Stadler R, Klebl F, Landouar-Arsivaud L, Lemoine R, Hedrich R,**
682 **Sauer N. 2005.** Arabidopsis POLYOL TRANSPORTER5, a new member of the
683 monosaccharide transporter-like superfamily, mediates H^+-Symport of numerous
684 substrates, including myo-inositol, glycerol, and ribose. *Plant Cell* **17**(1): 204-218.
685 **Klepek YS, Volke M, Konrad KR, Wippel K, Hoth S, Hedrich R, Sauer N. 2010.**
686 Arabidopsis thaliana POLYOL/MONOSACCHARIDE TRANSPORTERS 1 and 2:

687 fructose and xylitol/H^+ symporters in pollen and young xylem cells. *J Exp Bot* **61**(2):
688 537-550.
689 **Krasensky J, Jonak C. 2012.** Drought, salt, and temperature stress-induced metabolic
690 rearrangements and regulatory networks. *J Exp Bot* **63**(4): 1593-1608.
691 **Krieger E, Vriend G. 2014.** YASARA View - molecular graphics for all devices - from
692 smartphones to workstations. *Bioinformatics* **30**(20): 2981-2982.
693 **Lemoine R, Daie J, Wyse R. 1988.** Evidence for the Presence of a Sucrose Carrier in
694 Immature Sugar Beet Tap Roots *Plant Physiology* **86**(2): 575-580.
695 **Li C, Meng D, Piñeros MA, Mao Y, Dandekar AM, Cheng L. 2020.** A Sugar Transporter
696 Takes Up both Hexose and Sucrose for Sorbitol-Modulated In Vitro Pollen Tube
697 Growth in Apple. *The Plant Cell* **32**(2): 449.
698 **Michonneau P, Roblin G, Bonmort J, Fleurat-Lessard P. 2004.** Valine uptake in the tap
699 root of sugar beet: a comparative analysis with sucrose uptake. *J Plant Physiol*
700 **161**(12): 1299-1314.
701 **Minh BQ, Schmidt HA, Chernomor O, Schrempf D, Woodhams MD, von Haeseler A,**
702 **Lanfear R. 2020.** IQ-TREE 2: New Models and Efficient Methods for Phylogenetic
703 Inference in the Genomic Era. *Mol Biol Evol* **37**(5): 1530-1534.
704 **Newman IA. 2001.** Ion transport in roots: measurement of fluxes using ion-selective
705 microelectrodes to characterize transporter function. *Plant Cell Environ* **24**(1): 1-14.
706 **Nieberl P, Ehrl C, Pommerrenig B, Graus D, Marten I, Jung B, Ludewig F, Koch W,**
707 **Harms K, Flügge U-I, et al. 2017.** Functional characterisation and cell specificity of
708 BvSUT1, the transporter that loads sucrose into the phloem of sugar beet (*Beta*
709 *vulgaris* L.) source leaves. *Plant Biology* **19**(3): 315-326.
710 **Paulsen PA, Custódio TF, Pedersen BP. 2019.** Crystal structure of the plant symporter
711 STP10 illuminates sugar uptake mechanism in monosaccharide transporter
712 superfamily. *Nature Communications* **10**(1): 407.
713 **Pommerrenig B, Ludewig F, Cvetkovic J, Trentmann O, Klemens PAW, Neuhaus HE.**
714 **2018.** In Concert: Orchestrated Changes in Carbohydrate Homeostasis Are Critical for
715 Plant Abiotic Stress Tolerance. *Plant and Cell Physiology* **59**(7): 1290-1299.
716 **Poschet G, Hannich B, Raab S, Jungkunz I, Klemens PA, Krueger S, Wic S, Neuhaus**
717 **HE, Buttner M. 2011.** A novel Arabidopsis vacuolar glucose exporter is involved in
718 cellular sugar homeostasis and affects the composition of seed storage compounds.
719 *Plant Physiol* **157**(4): 1664-1676.
720 **Reinders A, Panshyshyn JA, Ward JM. 2005.** Analysis of transport activity of Arabidopsis
721 sugar alcohol permease homolog AtPLT5. *J Biol Chem* **280**(2): 1594-1602.
722 **Reinders A, Sivitz AB, Ward JM. 2012.** Evolution of plant sucrose uptake transporters.
723 *Front Plant Sci* **3**: 22.
724 **Reyer A, Häßler M, Scherzer S, Huang S, Pedersen JT, Al-Rasheid KAS, Bamberg E,**
725 **Palmgren M, Dreyer I, Nagel G, et al. 2020.** Channelrhodopsin-mediated
726 optogenetics highlights a central role of depolarization-dependent plant proton pumps.
727 *Proceedings of the National Academy of Sciences* **117**(34): 20920-20925.
728 **Riesmeier JW, Willmitzer L, Frommer WB. 1992.** Isolation and characterization of a
729 sucrose carrier cDNA from spinach by functional expression in yeast. *EMBO J*
730 **11**(13): 4705-4713.
731 **Rodrigues CM, Müdsam C, Keller I, Zierer W, Czarnecki O, Corral JM, Reinhardt F,**
732 **Nieberl P, Fiedler-Wiechers K, Sommer F, et al. 2020.** Vernalization Alters Sink
733 and Source Identities and Reverses Phloem Translocation from Taproots to Shoots in
734 Sugar Beet. *The Plant Cell* **32**(10): 3206-3223.
735 **Rodrigues CM, Mudsam C, Keller I, Zierer W, Czarnecki O, Corral JM, Reinhardt F,**
736 **Nieberl P, Fiedler-Wiechers K, Sommer F, et al. 2020.** Vernalization Alters Sink

and Source Identities and Reverses Phloem Translocation from Taproots to Shoots in Sugar Beet. *Plant Cell* **32**(10): 3206-3223.

Rottmann T, Fritz C, Sauer N, Stadler R. 2018. Glucose Uptake via STP Transporters Inhibits in Vitro Pollen Tube Growth in a HEXOKINASE1-Dependent Manner in Arabidopsis thaliana. *Plant Cell* **30**(9): 2057-2081.

Rottmann T, Zierer W, Subert C, Sauer N, Stadler R. 2016. STP10 encodes a high-affinity monosaccharide transporter and is induced under low-glucose conditions in pollen tubes of Arabidopsis. *J Exp Bot* **67**(8): 2387-2399.

Saftner RA, Daie J, Wyse RE. 1983. Sucrose Uptake and Compartmentation in Sugar Beet Taproot Tissue *Plant Physiology* **72**(1): 1-6.

Saftner RA, Wyse RE. 1980. Alkali Cation/Sucrose Co-transport in the Root Sink of Sugar Beet. *Plant Physiology* **66**(5): 884-889.

Sakr S, Lemoine R, Gaillard C, Delrot S. 1993. Effect of cutting on solute uptake by plasma membrane vesicles from sugar beet (*Beta vulgaris* L.) leaves. *Plant Physiol* **103**(1): 49-58.

Sauer N, Friedlander K, Graml-Wicke U. 1990. Primary structure, genomic organization and heterologous expression of a glucose transporter from *Arabidopsis thaliana*. *EMBO J* **9**(10): 3045-3050.

Sauer N, Tanner W. 1989. The hexose carrier from Chlorella. cDNA cloning of a eucaryotic H^+-cotransporter. *FEBS Lett* **259**(1): 43-46.

Schneider S, Hulpke S, Schulz A, Yaron I, Holl J, Imlau A, Schmitt B, Batz S, Wolf S, Hedrich R, et al. 2012. Vacuoles release sucrose via tonoplast-localised SUC4-type transporters. *Plant biol (Stuttg)* **14**(2): 325-336.

Schneider S, Schneidereit A, Konrad KR, Hajirezaei MR, Gramann M, Hedrich R, Sauer N. 2006. Arabidopsis INOSITOL TRANSPORTER4 mediates high-affinity H^+ symport of myoinositol across the plasma membrane. *Plant Physiol* **141**(2): 565-577.

Schneider S, Schneidereit A, Udvardi P, Hammes U, Gramann M, Dietrich P, Sauer N. 2007. Arabidopsis INOSITOL TRANSPORTER2 mediates H^+ symport of different inositol epimers and derivatives across the plasma membrane. *Plant Physiol* **145**(4): 1395-1407.

Scholz-Starke J, Buttner M, Sauer N. 2003. AtSTP6, a new pollen-specific H^+-monosaccharide symporter from Arabidopsis. *Plant Physiol* **131**(1): 70-77.

Schulz A, Beyhl D, Marten I, Wormit A, Neuhaus E, Poschet G, Buttner M, Schneider S, Sauer N, Hedrich R. 2011. Proton-driven sucrose symport and antiport are provided by the vacuolar transporters SUC4 and TMT1/2. *Plant J* **68**(1): 129-136.

Tarkowski LP, Van den Ende W. 2015. Cold tolerance triggered by soluble sugars: a multifaceted countermeasure. *Front Plant Sci* **6**: 203.

Wang Z, Wei X, Yang J, Li H, Ma B, Zhang K, Zhang Y, Cheng L, Ma F, Li M. 2020. Heterologous expression of the apple hexose transporter MdHT2.2 altered sugar concentration with increasing cell wall invertase activity in tomato fruit. *Plant biotechnology journal* **18**(2): 540-552.

Wanner LA, Junttila O. 1999. Cold-induced freezing tolerance in Arabidopsis. *Plant Physiol* **120**(2): 391-400.

Wittek A, Dreyer I, Al-Rasheid KAS, Sauer N, Hedrich R, Geiger D. 2017. The fungal UmSrt1 and maize ZmSUT1 sucrose transporters battle for plant sugar resources. *J Integr Plant Biol* **59**(6): 422-435.

Wormit A, Trentmann O, Feifer I, Lohr C, Tjaden J, Meyer S, Schmidt U, Martinoia E, Neuhaus HE. 2006. Molecular identification and physiological characterization of a novel monosaccharide transporter from Arabidopsis involved in vacuolar sugar transport. *Plant Cell* **18**(12): 3476-3490.

Wyse R. 1979. Sucrose Uptake by Sugar Beet Tap Root Tissue. *Plant Physiology* **64**(5): 837-841.

Figures

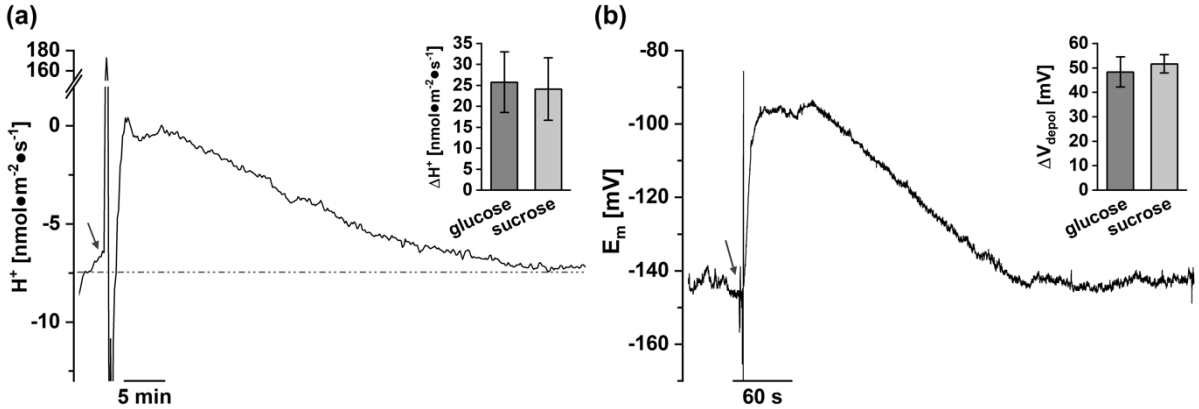

Fig. 1 Glucose- and sucrose-induced changes in H^+ fluxes and membrane depolarization of *Beta vulgaris* taproot cells. (a) H^+ flux trace recorded from taproot slices in response to 50 mM glucose treatment. Time of glucose application is denoted by the arrow. Negative and positive fluxes represent H^+ release from the cells and H^+ uptake into the cells, respectively. The H^+ flux level determined at rest shortly before sugar administration is indicated by a dotted line. The bar graph shows the maximal glucose- and sucrose-induced changes in the H^+ fluxes relative to the H^+ flux level at rest. Data represent means ± SEM with n = 11 each for glucose and sucrose. (b) Free running membrane voltage trace recorded from a taproot slice in response to 50 mM glucose. Time of glucose application is indicated by the arrow. The bar graph shows the maximal glucose- and sucrose-induced depolarization of the slices. Data represent means ± SEM of seven or six different taproots for glucose and sucrose, respectively. In (a), (b) taproots from GT2 were used.

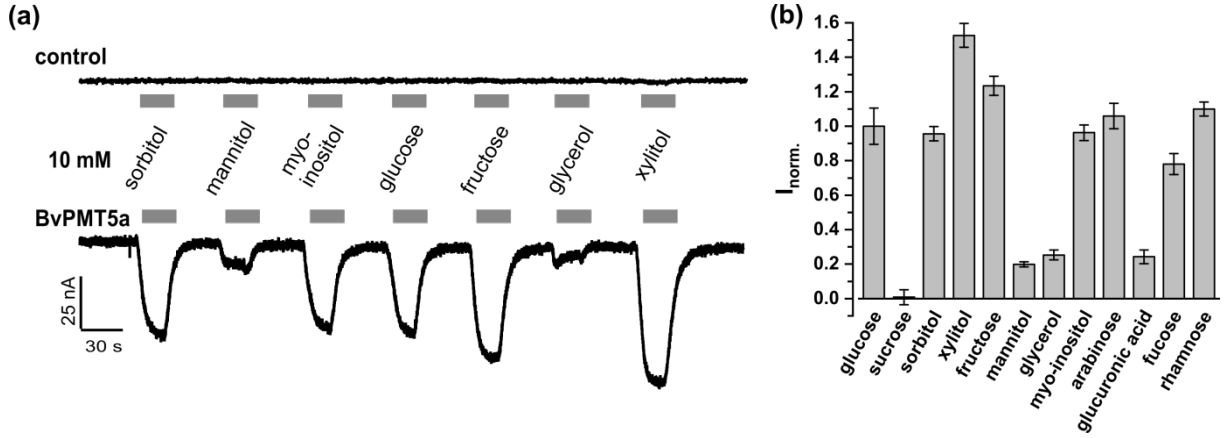

Fig. 2 Substrate specificity of BvPMT5a. (a) Representative macroscopic current recordings of *Xenopus laevis* oocytes injected either with water (control) or BvPMT5a complementary RNA. Currents were recorded at a membrane potential of -40 mV and at pH 5.5 during a 30 s application (grey bar) of different sugar compounds (10 mM). Downward deflections indicate inward currents. (b) Current responses of BvPMT5a-expressing oocytes to the application of different sugar compounds (10 mM). The respective responses of each oocyte were normalized to the glucose-induced change in the inward currents of that oocyte. Data represents means ± SEM of 6 to 36 individual oocytes.

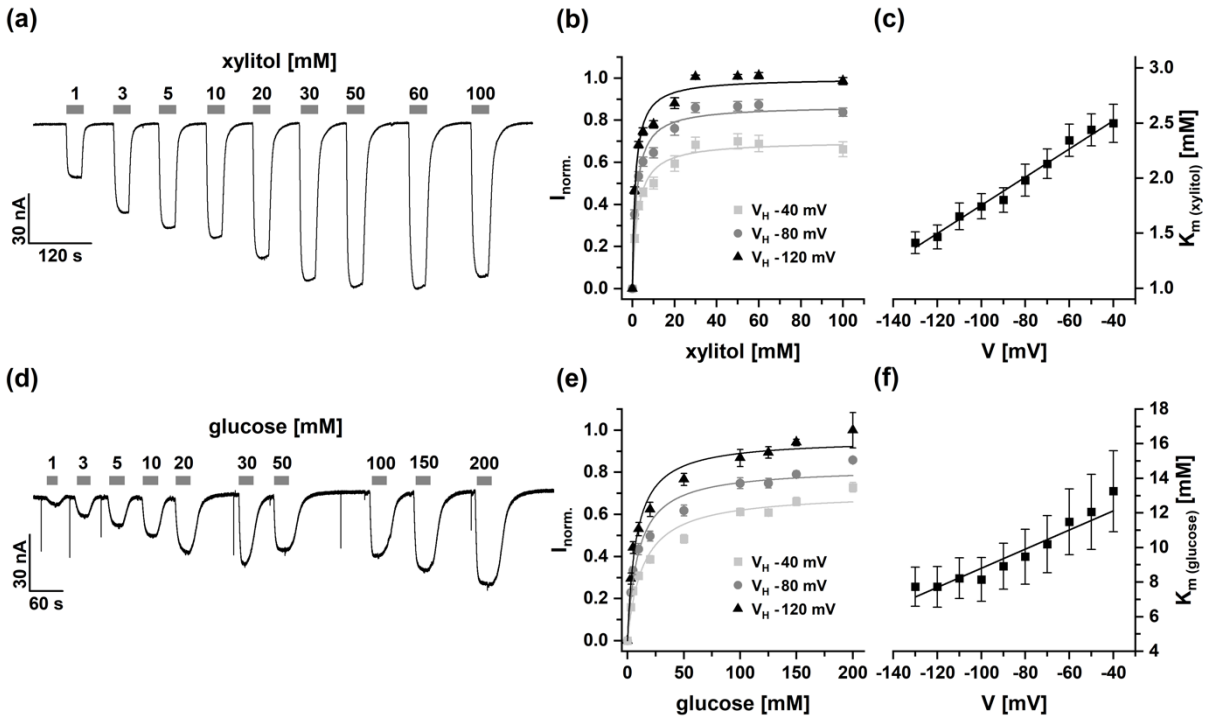

Fig. 3 Xylitol- and glucose-dose dependency of BvPMT5a. (a, d) Current responses of BvPMT5a-expressing oocytes to xylitol (a) or glucose (d) application at the indicated concentrations. The duration of the substrate administration is indicated by the grey bar above the current trace. Currents were recorded at a membrane voltage of -40 mV at pH 5.5. (b), (e), Xylitol- or- glucose-dependent currents plotted as a function of the substrate concentration. Currents were recorded at the membrane voltages as indicated and pH 5.5. Recorded currents were normalized to the maximum current recorded at a membrane voltage of -120 mV. The solid line gives the best fit of the data set with a Michaelis-Menten function. (c, f) Voltage dependency of the K_m values. K_m values derived from the best Michaelis-Menten-fits as shown in (b, e) were plotted against the respective membrane voltages. In (b, c) and (e, f) data represents means ± SEM of 9 and 10 individual oocytes, respectively.

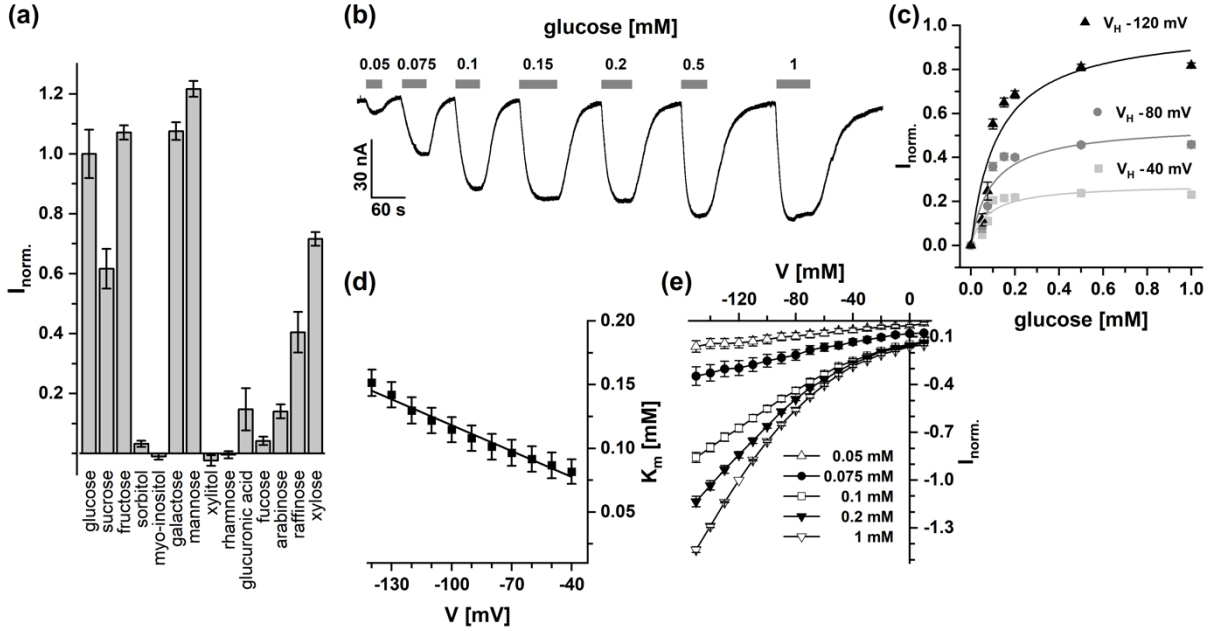

Fig. 4 Substrate specificity, glucose-dose and voltage dependency of BvSTP13. (a) Current responses of BvSTP13-expressing oocytes to the application of different sugar compounds (10 mM) recorded at a membrane voltage of -40 mV. The respective responses of each oocyte were normalized to the glucose-induced change in the inward currents of that oocyte. Data represents means ± SEM of 7 to 24 individual oocytes. (b) Representative current responses of BvSTP13-expressing oocytes to glucose application at the indicated concentrations. The duration of glucose administration is indicated by the grey bar above the current trace. Currents were recorded at a membrane voltage of -40 mV at pH 5.5. Noise peaks generated during the perfusion were dimmed offline. (c) Glucose-dependent BvSTP13-mediated currents plotted as a function of the substrate concentration. Currents were recorded at the membrane voltages indicated and pH 5.5. Recorded currents were normalized to the maximum current recorded at a membrane voltage of -120 mV. The solid line gives the best fit of the data set with a Michaelis-Menten function. (d) Voltage dependency of the K_m values. K_m values derived from the best Michaelis-Menten-fits as shown in C were plotted against the respective membrane voltages. (e) Current-voltage curves recorded at pH 5.5 under glucose treatment at indicated concentrations. Currents measured were normalized to the response to 1 mM glucose measured at -120 mV. In (a-e) all experiments were conducted at pH 5.5. In (c-e) data represents means ± SEM of 12 individual oocytes.

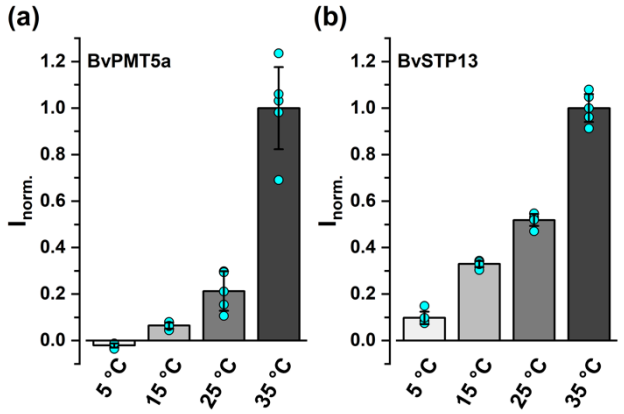

Fig. 5 Temperature dependency of BvPMT5a and BvSTP13. Current responses of BvPMT5a (a)- and BvSTP13 (b)-expressing oocytes to 50 or 0.5 mM glucose, respectively, measured at -140 mV and temperatures as indicated were normalized to those at 35 °C. A Q_{10} value of 3.97 ± 0.57 for BvPMT5a and 2.18 ± 0.64 for BvSTP13 (means ± SD, n = 5) was determined. Q_{10} values were calculated as mean factors between temperatures, which resulted in distinct currents in the range of 15 - 35 °C for BvPMT15 and 5 - 35 °C for BvSTP13 (mean ± SD of 5 individual oocytes). Turquoise circles indicate the individual data points.

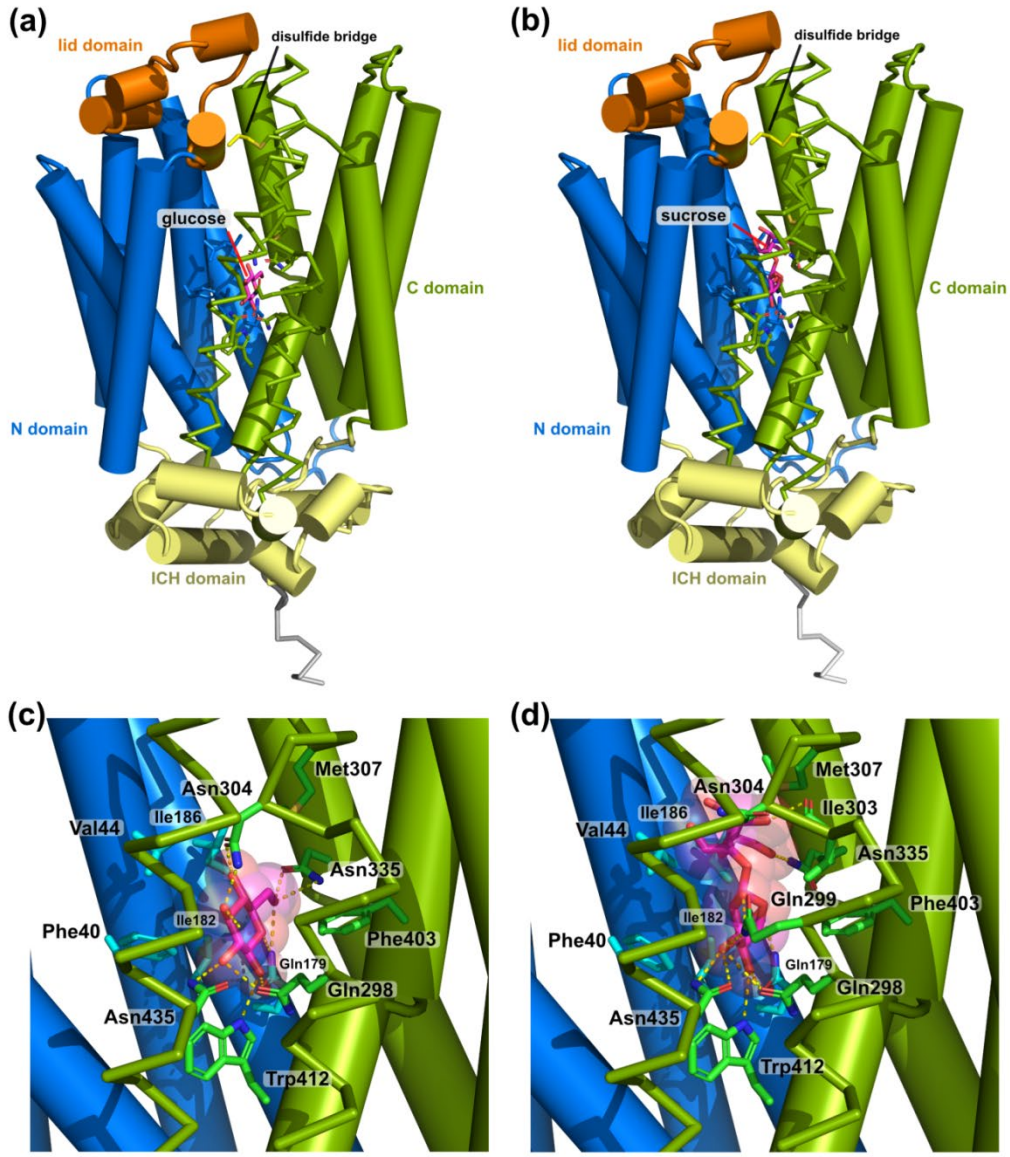

Fig. 6 Comparison of a BvSTP13 model bound to glucose and sucrose. (a) A BvSTP13 model with glucose bound in the saccharide binding site. (b) BvSTP13 3D model bound to sucrose. The BvSTP13 model follows the color-coding scheme to indicate the different domains as stated in Fig. S8. The saccharide moieties are shown as stick representation with their carbon atoms colored in magenta and the oxygen atoms marked in red. (c) An enlargement of the binding site in the interaction of BvSTP13 with glucose is shown. Residues in close proximity (≤ 5 Å) are shown as sticks, hydrogen bonds between the glucose molecule and residues of BvSTP13 are indicated by stippled lines colored in yellow. (d) The binding site of a BvSTP13 model interacting with sucrose is shown (magnification). The sucrose molecule was docked into the saccharide binding site of our BvSTP13 homology model such that the glucose moiety of the sucrose occupied the same position as the glucose molecule in the AtSTP10

870 structure. Energy minimization was performed, and a 10 ns MD trajectory was calculated
871 with BvSTP13 placed in a bilayer membrane and the extra- and intracellular part surrounded
872 by water. The model shows that the glucose moiety of the sucrose molecule can engage in
873 similar hydrogen bonds as the glucose in the BvSTP13-glucose model. Furthermore, the
874 fructose moiety of the sucrose molecule can form hydrogen bonds for instance with the
875 carbonyl of Ile303 and with the carboxyamide group of Asn335.
876
877
878 **Supporting Information**
879
880 **Fig. S1.** Cellular loading of esculin in taproot cells.
881
882 **Fig. S2.** Sucrose-induced changes in H^+ fluxes and membrane depolarization of *Beta vulgaris*
883 taproot cells.
884
885 **Fig. S3.** Phylogenetic tree of PMTs and STPs of *Arabidopsis thaliana* (At) and *Beta vulgaris*
886 (Bt).
887
888 **Fig. S4.** Effect of low temperature on expression of *STP*- and *PMT*-like genes in *Beta*
889 *vulgaris* taproots.
890
891 **Fig. S5.** pH and voltage dependency of BvPMT5a.
892
893 **Fig. S6.** Sucrose-dose dependency and voltage dependency of BvSTP13.
894
895 **Fig. S7.** pH and voltage dependency of BvSTP13.
896
897 **Fig. S8.** Comparison of the 3D homology model of BvSTP13 model and the crystal structure
898 of AtSTP10.
899
900 **Fig. S9.** Structure guided alignment of sugar transporters.
901
902 **Methods S1** Esculin uptake in Beta vulgaris taproot cells
903

904 **Methods S2** Gene expression analysis

905

906 **Supporting References**

907